Journal of Power Sources 238 (2013) 180–189

Contents lists available at SciVerse ScienceDirect

Journal of Power Sources

journal homepage: www.elsevier.com/locate/jpowsour

Microwave-assisted hydrothermal annealing of binary Ni–Co oxy-hydroxides for asymmetric supercapacitors

Chi-Chang Hu*, Chun-Tsung Hsu, Kuo-Hsin Chang*, Hsiang-Yu Hsu

Laboratory of Electrochemistry and Advanced Materials, Department of Chemical Engineering, National Tsing-Hua University, No. 101, Section 2, Kuang-Fu Road, Hsin-Chu 30013, Taiwan

HIGHLIGHTS

- MAHA is promising in tuning the crystal phase/size of Ni–Co oxy-hydroxides at low temperatures in short time.
- The crystalline index quantifies the degree of phase transformation from Ni–Co hydroxides to NiCo2O4 crystals.
- The larger size of NiCo2O4 crystals is, the longer activation time is needed but higher reversibility is obtained.
- Importance of potential window for evaluating C_S of battery-like materials is demonstrated.

GRAPHICAL ABSTRACT

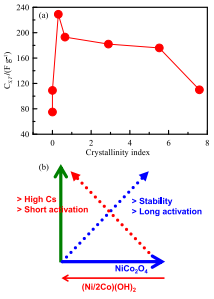

ARTICLE INFO

Article history:
Received 27 April 2012
Received in revised form
26 February 2013
Accepted 3 March 2013
Available online 26 March 2013

Keywords:
Nickel–cobalt oxy-hydroxide
Crystal phase
Crystal size
Microwave-assisted hydrothermal annealing
Asymmetric supercapacitor

ABSTRACT

Binary nickel–cobalt oxy-hydroxides (denoted as NCOH) with tunable crystal phases are prepared from an atomic mixture of $Ni(OH)_2$ + $Co(OH)_2$ in the 1:2 ratio (denoted as $(Ni/2Co)(OH)_2$) through a microwave-assisted hydrothermal annealing (MAHA) method. The $(Ni/2Co)(OH)_2$ powders are synthesized through a sol–gel process from an aqueous solution containing $NiCl_2 \cdot 6H_2O$ and $CoCl_2 \cdot 6H_2O$. The MAHA process is demonstrated to be a novel and promising method for transforming/tuning the crystal phase and size of NCOH at relatively low annealing temperatures in short time. The MAHA temperature and time are varied to transform the crystalline phases from a hydroxide mixture to $NiCo_2O_4$ nanocrystals, which can be quantified by a crystalline index (denoted as *CI*) value obtained from X-ray diffraction (XRD) patterns. The higher content and larger size of $NiCo_2O_4$ nanocrystals are, the longer electrochemical activation time is needed. The rate of phase transformation can be enhanced by adding microwave adsorbents, graphene oxide (GO), to obtain a $NiCo_2O_4$/RGO composite with reduced crystal size (RGO: reduced GO). The variation in the crystalline index and the effect of the potential window on the specific capacitance of NCOH powders are systematically compared and discussed in this work.

1. Introduction

Nickel and cobalt oxides and hydroxides have attracted considerable research interest in the electrochemical energy storage systems such as rechargeable batteries [1–3] and asymmetric supercapacitors [4–6] because of their promising redox properties in the high positive potential region (above 1.3 V vs. reversible

* Corresponding authors. Tel./fax: +886 3 573 6027.
E-mail addresses: cchu@che.nthu.edu.tw (C.-C. Hu), khchang@mx.nthu.edu.tw (K.-H. Chang).

0378-7753/$ – see front matter © 2013 Elsevier B.V. All rights reserved.
http://dx.doi.org/10.1016/j.jpowsour.2013.03.019

hydrogen electrode, RHE) [7]. However, the requirements for rechargeable batteries and asymmetric supercapacitors are basically different [8–10]. Due to the high power and long cycle-life characteristics of supercapacitors [8,10], electronic and ionic conductivities, electrochemical reversibility, and degradation mechanisms of electrode materials have to be simultaneously considered [11]. In addition, how to design ideal microstructures of electrochemically active materials in order to enhance the utilization of the surface redox couples for pseudocapacitors is an important topic in this field. For rechargeable batteries, the energy density of devices is usually enhanced by utilizing the bulk phase of oxides or hydroxides [9,12] although power-oriented rechargeable batteries [13–15] have attracted considerable attention and have been developed for hybrid and pure electric vehicles (EV and EV) recently. On the other hand, all the above reports reveal the great interest in synthesizing nickel–cobalt oxides and hydroxides in various forms or microstructures for the electrochemical energy storage applications.

One of the key factors determining the electrochemical performances of nickel and cobalt oxides/hydroxides is their crystalline structure which is important to the utilization, electronic conductivity and ion-diffusion rate of resultant materials [16,17], affecting the electrochemical reversibility of redox couples. For instance, the electrochemical reversibility and electrochemically active surface area of Ni and Co oxides/hydroxides have been reported to change by adding foreign cations due to the crystal distortion [18–20]. In addition, spinel nickel cobaltite ($NiCo_2O_4$) has been reported to possess a much better electronic conductivity, at least two orders of magnitude higher, and higher specific capacitance than those of nickel and cobalt oxides [17]. Therefore, how to effective control the phase transformation between Ni–Co hydroxides and nickel cobaltite and to obtain suitable microstructures of resultant Ni–Co oxy-hydroxides for electrochemical energy storage systems are of both academic and practical interests.

In general, nickel–cobalt hydroxides can be simply prepared by means of the sol–gel process [5,7] and the phase transformation from hydroxides to oxides can be simply done by annealing in air through controlling the annealing time and temperature [5,7,21–23]. However, when the bridging oxo bonds among hydroxides are formed and crystals are grown via annealing due to thermal sintering, the specific capacitance of resultant oxides will decrease very sharply because of the loss in the electroactive sites [11,16,17]. Therefore, hydrothermal annealing was proposed to independently control the crystal size and water content of $RuO_2 \cdot xH_2O$ nanocrystals in our previous work [24–26]. However, hydrothermal annealing is a time-wasting process while this drawback can be overcome using the microwave heating. Moreover, the heating mode may be significantly affected by the solvents with different microwave-absorption index. Hence, this work tries to develop a simple microwave-assisted hydrothermal annealing (MAHA) process to control the phase transformation of Ni–Co hydroxides for identifying the important influences of crystalline phase and size of Ni–Co oxy-hydroxides on the asymmetric supercapacitor performances. Finally, graphene oxide (GO) added in the hydroxides mixture is used to efficiently absorb microwave [27] in order to further promote the phase transformation rate. Moreover, a composite consisting of homogeneously dispersed $NiCo_2O_4$ nanocrystals on reduced GO (RGO) shows excellent performances for the asymmetric supercapacitors.

2. Experimental

2.1. Preparation of Ni–Co oxy-hydroxide and electrode preparation

The binary Ni–Co hydroxide mixture was prepared by means of a modified sol–gel process [7]. $NiCl_2 \cdot 6H_2O$ and $CoCl_2 \cdot 6H_2O$ in a molar ratio of 1:2 were dissolved and agitated in a solution with equal volumes of water and ethanol to form organometallic species at room temperature for 30 min. A 1 M NaOH solution was then added into the stirred solution until hydroxide precipitates were clearly found (pH >8). The hydroxide precipitates could be easily obtained by means of a centrifuge, which was washed with pure water several times until the pH was close to 7. Some precipitates were dried in a vacuum oven at room temperature for 8 h. The other precipitates were well-dispersed in de-ionized water in an ultrasonic bath for 20 min and then annealed in a microwave reactor (CEM, USA) at 100, 150, 200, and 210 °C for 15 min for obtaining Ni–Co oxy-hydroxide powders (denoted as NCOH100, NCOH150, NCOH200, and NCOH210, respectively). These MAHA-treated oxide powders were well-dispersed in de-ionized water in an ultrasonic bath for 20 min and dropped onto pretreated graphite substrates without any binder. These electrodes were dried in a vacuum oven at 85 °C overnight. The loading of oxy-hydroxides, 0.50 ± 0.03 mg cm^{-2}, is the weight difference before and after the oxy-hydroxide coating, which can be effectively controlled by the number of drops. The graphite substrates were first abraded with ultrafine SiC paper, rinsed with acetone and water, then cleaned in a 0.1 M HCl solution at room temperature (ca. 26 °C) for 10 min, and finally degreased with water in an ultrasonic bath. The exposed geometric area of these pretreated graphite supports was equal to 1 cm^2, while the other surface areas were insulated with polytetrafluorene ethylene coatings.

2.2. Characterization

Cyclic voltammograms (CV) and chronopotentiograms (CP) under the three- and two-electrode modes were measured by an electrochemical analyzer (CHI633c, CH Instruments Inc.) in 1 M NaOH (Hanawa EP, Japan). The reference and counter electrodes were Ag/AgCl (Argenthal, 3 M KCl, 0.207 V vs. SHE at 25 °C) and a piece of platinum gauze (99.95%, 0.5 mm in diameter), respectively. A Luggin capillary with its tip being covered with a conductive membrane was used to minimize errors due to *iR* drop in the electrolyte. X-ray diffraction patterns were obtained from an X-ray powder diffractometer (CuK_α, Ultima IV, Rigaku). The crystalline index of various Ni–Co oxy-hydroxide powders, i.e., the crystal size ratio of hydroxide-to-$NiCo_2O_4$, was deduced from the crystal size data estimated with the Debye–Scherrer equation from facets (101) and (311) of $(Ni/2Co)(OH)_2$ and $NiCo_2O_4$, respectively. The morphology and nanostructures of $NiCo_2O_4$ nanocrystals uniformly dispersed onto reduced graphene oxide (RGO) nanosheets were examined by a high-resolution transmission electron microscope (HR-TEM, JEM-2010, Joel).

All solutions used in this work were prepared with deionized water produced by a reagent water system (Milli-Q SP, Japan) at 18 MΩ cm. All reagents, not specified, without further purification are Merck, GR. The electrolyte, 1 M NaOH, used for electrochemical characterization was maintained at 25 °C and degassed with purified N_2 for 25 min before measurements. This nitrogen was passed over the solutions during the measurements. The solution temperature was maintained at the specified temperature by a water thermostat (Haake DC3 and K20).

3. Results and discussion

3.1. Effect of the MAHA temperature

The rate of phase transformation of hydroxides is significantly affected by changing the MAHA temperature, probably due to a change in the steam pressure because the microwave power was kept constant (100 W) during all MAHA procedures. Note that the

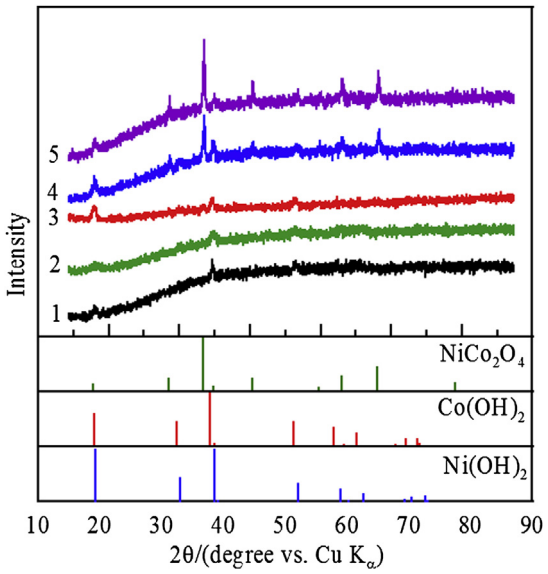

Fig. 1. XRD patterns of (1) $(Ni/2Co)(OH)_2$, (2) NCOH100, (3) NCOH150, (4) NCOH200 and (5) NCOH210 prepared by microwave-assisted hydrothermal annealing for 15 min.

as-prepared precipitates can be identified as a homogeneous mixture of $Ni(OH)_2$ and $Co(OH)_2$ under the atomic level (denoted as $(Ni/2Co)(OH)_2$, see below) although the intensities of all diffraction peaks are not high on pattern 1 in Fig. 1. This is the common property of sol–gel-derived hydroxides without annealing [26,28]. From pattern 2, no diffraction peaks corresponding to $NiCo_2O_4$ can be clearly identified meanwhile peak broadening of the original diffraction peaks is visible, suggesting insignificant phase transformation and some damages on the crystalline structure of $(Ni/2Co)(OH)_2$ although some bridging oxo bonds may be formed between hydroxide precipitates. This phenomenon is attributable to that the formation of $NiCo_2O_4$ crystallites needs a nucleation step which usually requires higher activation energy in comparing with the formation of the oxo bonds. When the MAHA temperature is equal to 150 °C, two vague $NiCo_2O_4$ peaks located at $2\theta = 36.70$ and 64.98° can be found on pattern 3. When the MAHA temperatures are equal to/above 200 °C, several diffraction peaks corresponding to $NiCo_2O_4$ are clearly found meanwhile hydroxide peaks are also visible (see patterns 4 and 5 in Fig. 1). Obviously, the resultant materials are a mixture, at least, consisting of $NiCo_2O_4$ and $(Ni/2Co)(OH)_2$, which is consequently named as Ni–Co oxy-hydroxides (i.e., NCOH). Interestingly, there is no peak corresponding to NiO or CoO, indicating that $NiCo_2O_4$ is the preferred crystalline phase by using the MAHA method. The oxygen molecules dissolved in the deionized water are believed to be responsible for the oxidation of Co(II) into Co(III) during the MAHA process, favorable for the formation of $NiCo_2O_4$.

Fig. 2 shows the TEM microstructures of all Ni–Co oxy-hydroxides examined in Fig. 1. The as-prepared precipitates are porous aggregates of $(Ni/2Co)(OH)_2$ primary nanoparticles although these porous aggregates with their size in sub-micrometer do not show any regular shape. From a comparison of Fig. 2a–c, relatively dense aggregates are clearly found when the as-prepared samples were subjected to MAHA (e.g., see the dark parts in Fig. 2b). The original, sub-micrometer, aggregated morphology is not visible in Fig. 2b meanwhile some spherical and dense particulates around 30 nm are visible in Fig. 2c (observed under a higher magnification for 50 primary nanoparticles), attributed to the formation of $NiCo_2O_4$ nanocrystals although the XRD peaks corresponding to $NiCo_2O_4$ nanocrystals are not clear on pattern 3 in Fig. 1, probably due to the tiny size of crystallites and/or the poor crystalline quality of resultant $NiCo_2O_4$. When the MAHA temperature is equal to/above 200 °C, the size and number of the spherical and dense particles are enlarged and increased simultaneously. The average size of these spherical $NiCo_2O_4$ particulates is 30.2, 43.3, and 57.4 nm when the MAHA temperature is equal to 150, 200, and 210 °C, respectively. Since the crystal size estimated from the diffraction peak, $NiCo_2O_4$ (311) facet, in Fig. 1 is much smaller than that observed by means of TEM, the spherical particulates are considered as aggregates of $NiCo_2O_4$ nanocrystals. Note that some ambiguous and irregular aggregates and particles corresponding to the original Ni–Co hydroxides are still visible in Fig. 2b–e, revealing that the powders with the MAHA treatment are mixtures of $NiCo_2O_4$ and $(Ni/2Co)(OH)_2$.

Fig. 3 shows the typical cyclic voltammograms measured in 1 M NaOH for all Ni–Co oxy-hydroxides prepared in this section. In fact, this electrochemical test is called as an electrochemical activation process which is used to activate the surface oxy-hydroxyl-metal species (superficial redox sites) by using CV cycling between 0.95 and 1.6 V (vs. RHE) at 25 mV s^{-1} for 150 cycles [7] in this work. From a comparison of all CV curves, several features need to be mentioned. First, for the as-prepared $(Ni/2Co)(OH)_2$ powders, the voltammetric current density gradually decreases with prolonging the potential cycling (see Fig. 3a). This result indicates that the binary hydroxide only needs few CV cycles to activate the redox species for the charge storage/delivery and that the binary hydroxide is not very stable in this 150-cycle test. Second, the CV curves approximately follow the same trace in the whole potential region for the NCOH100 powders. This result indicates that NCOH100 can be completely activated within 50 CV cycles of electrochemical activation. Moreover, this material shows better electrochemical stability for the charge storage/delivery in this 150-cycle activation process in comparison with $(Ni/2Co)(OH)_2$. Third, the enhancement in the peak current density and voltammetric charges by this activation process is more obvious with increasing the MAHA temperature from a comparison of all curves in Fig. 3c–e. These results indicate that $NiCo_2O_4$ crystallites within NCOH150, NCOH200, and NCOH210 need an activation process longer than 150 cycles in order to completely activate all electroactive species. Moreover, the larger crystal size of $NiCo_2O_4$ is (obtained at a higher MAHA temperature), the larger enhancement (in proportion) of the peak current density and charges is obtained (e.g., see Fig. 3d and e). Fourth, the anodic peak potential of the redox couple is positively shifted from 1.29 V to ca. 1.39 V with increasing the MAHA temperature. This phenomenon is also visible for the cathodic peak on the negative sweeps. The above positive shift in the redox peak potentials is reasonably attributed to the formation and growth of $NiCo_2O_4$ nanocrystals at a higher MAHA temperature. Fifth, the specific capacitance deduced from the voltammetric charge on the negative sweeps of CVs reaches a maximum value at the MAHA temperature equal to 150 °C. This result suggests that the utilization of electroactive species strongly depends on the crystalline structure and crystal size of Ni–Co oxy-hydroxides.

The above results and discussion indicate that the co-existence of $NiCo_2O_4$ and $(Ni/2Co)(OH)_2$ at certain ratios reasonably enhances the utilization of the active materials (including $NiCo_2O_4$ and hydroxides) although the hydroxide species might be considered as impurities in the above mixture if $NiCo_2O_4$ is the desired product. Note that from Fig. 3a, the voltammetric behavior of the as-prepared hydroxide precipitates does not simply show the combined characteristics of $Ni(OH)_2$ and $Co(OH)_2$ (i.e., CVs containing several pairs of redox peaks at different potentials corresponding to the redox transitions of pure $Ni(OH)_2$ and $Co(OH)_2$ [3,7,29]). This phenomenon suggests that $Ni(OH)_2$ and $Co(OH)_2$ within the as-prepared sample is uniformly mixed under the atomic scale, which is reasonably denoted as $(Ni/2Co)(OH)_2$. Accordingly, MAHA

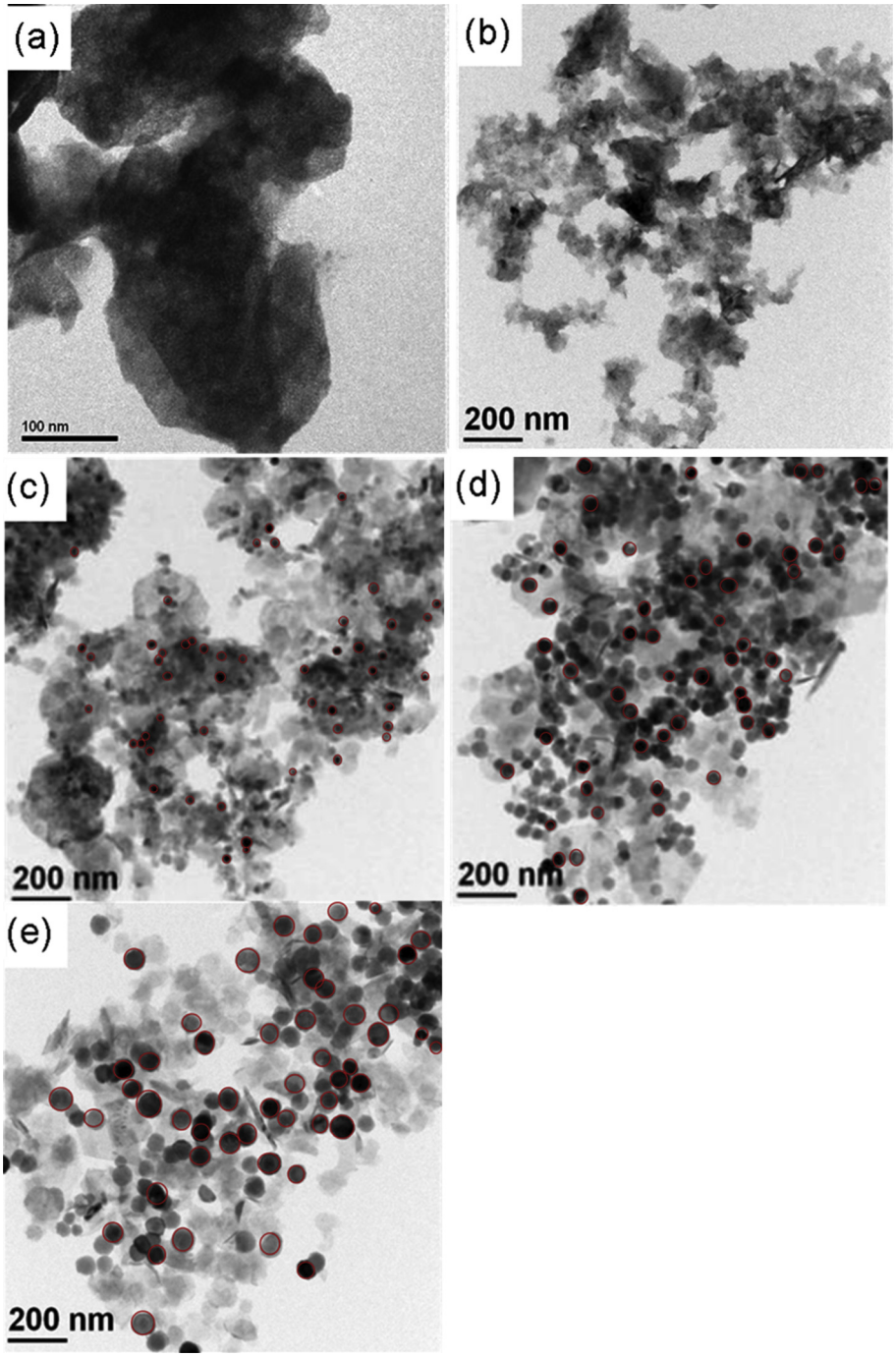

Fig. 2. Bright-field TEM images of (a) $(Ni/2Co)(OH)_2$, (b) NCOH100, (c) NCOH150, (d) NCOH200 and (e) NCOH210.

is an interesting tool which partially transforms $(Ni/2Co)(OH)_2$ into $NiCo_2O_4$ by varying the MAHA temperature or time (see below). Due to the consistent metallic composition between $NiCo_2O_4$ and $(Ni/2Co)(OH)_2$, the dispersion of $NiCo_2O_4$ nanocrystals in the $(Ni/2Co)(OH)_2$ impurity should be uniform. Therefore, the well dispersed $NiCo_2O_4$ nanocrystals surrounded with $(Ni/2Co)(OH)_2$ impurities may exhibit synergistic effects in reducing the peak potential difference and promoting the utilization of active materials although the CV activation cycle has to be increased due to the growth of $NiCo_2O_4$ nanocrystals.

Fig. 4a shows the typical charge–discharge curves measured at 5 mA cm^{-2} for various NCOH prepared in this section. From these CP curves obtained under the three-electrode mode, there is a charge plateau and a discharge plateau at ca. 0.2–0.27 and 0.23–0.15 V, respectively, indicating its battery-like behavior. In addition, the order of NCOH with respect to decreasing the specific capacitance is NCOH150 (C_S = 215 F g^{-1}) > NCOH200 (C_S = 150 F g^{-1}) > NCOH210 (C_S = 135 F g^{-1}) > $(Ni/2Co)(OH)_2$ (C_S = 95 F g^{-1}) > NCOH100 (C_S = 70 F g^{-1}). These results are consistent with the trend obtained from the CV study. Since the *iR* drops of all NCOH measured at different charge–discharge current densities are very similar (e.g., 5.9, 5.2, and 5.6 mV for NCOH210, NCOH150, and $(Ni/2Co)(OH)_2$, respectively measured at 5.0 mA), the electronic conductivity of $(Ni/2Co)(OH)_2$ was not significantly

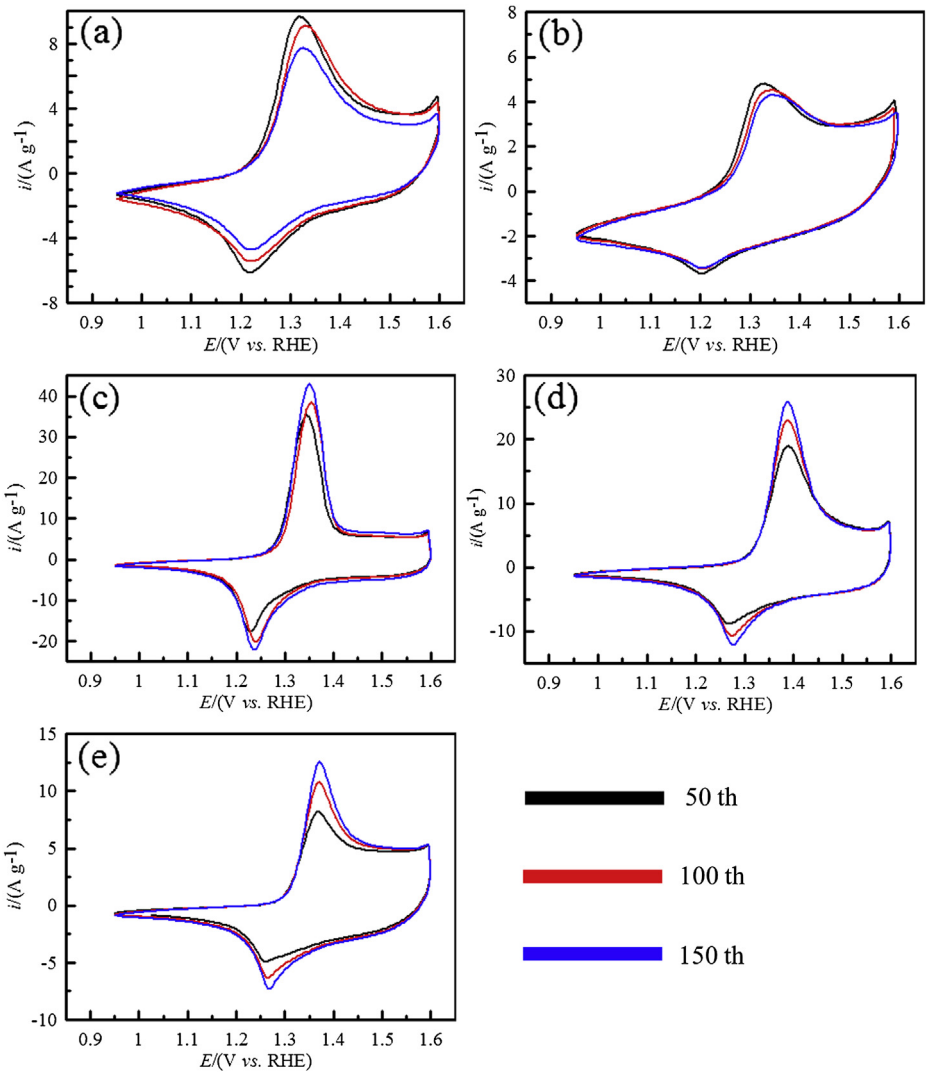

Fig. 3. The (1) 50th, (2) 100th, and (3) 150th cycles of CV curves for (a) $(Ni/2Co)(OH)_2$, (b) NCOH100, (c) NCOH150, (d) NCOH200 and (e) NCOH210 measured in 1 M NaOH at 25 mV s^{-1}.

improved by the partial phase transformation from hydroxides into $NiCo_2O_4$. Hence, the increase in the specific capacitance of NCOH150 is not attributable to the effect of electronic conductivity. Also note that the charge–discharge curves of all NCOH are not as symmetric as those of hydrous RuO_2 [25,26] or MnO_x [30] while their electrochemical reversibility is much better than that of $Ni(OH)_2$ [3,31]. Accordingly, these NCOH are proposed to be suitable for the electrode materials of a supercapacitor in the asymmetric design since the double-layer responses of the carbon-based negative electrodes will improve the charge–discharge performances of a full cell in such an asymmetric design [31].

The typical charge–discharge curves of an asymmetric supercapacitor with a NCOH150 positive electrode and an activated-carbon negative electrode are shown in Fig. 4b. Clearly, the charge–discharge curves become relatively asymmetric when the cell voltage is above 1.7 V. The relatively asymmetric response originates from the irreversible charge–discharge behavior of NCOH150 as the electrode potentials are positive than 0.52 V vs. Ag/AgCl (i.e., 1.57 V vs. RHE; see Fig. 4c). Based on this cell voltage, the energy and power densities of this asymmetric cell can be evaluated by varying the charge–discharge current density from 2 to 40 A g^{-1} (see Fig. 4d). On the basis of the total mass of the electrode materials on both electrodes, the energy and power densities of this device in the asymmetric design obtained at 2 A g^{-1} are equal to 17.8 Wh kg^{-1} and 1.8 kW kg^{-1}, respectively, which respectively decrease and increase to 9.0 Wh kg^{-1} and 36 kW kg^{-1} when the charge–discharge current density was increased to 40 A g^{-1}. Hence, Ni–Co oxy-hydroxides are suitable for the electrode materials of the asymmetric supercapacitors.

3.2. Effects of the MAHA time

The effects of varying the MAHA time on the phase transformation and crystal size of $NiCo_2O_4$ particulates were examined by the X-ray diffraction (XRD) analysis and typical results are shown in Fig. 5. Clearly, all XRD patterns reveal the coexistence of hydroxide and $NiCo_2O_4$, indicating that the phase transformation from $(Ni/2Co)(OH)_2$ to $NiCo_2O_4$ is very fast when the MAHA temperature is elevated (e.g., 210 °C in this case). However, hydroxides are the predominant phase on pattern 1 while $NiCo_2O_4$ becomes the main phase when the MAHA time is equal to/longer than 10 min (see patterns 2 and 3 in Fig. 5). Moreover, the Debye–Scherer equation was used to estimate the average crystal size. From patterns 1–3, the crystal size of $NiCo_2O_4$ gradually increases

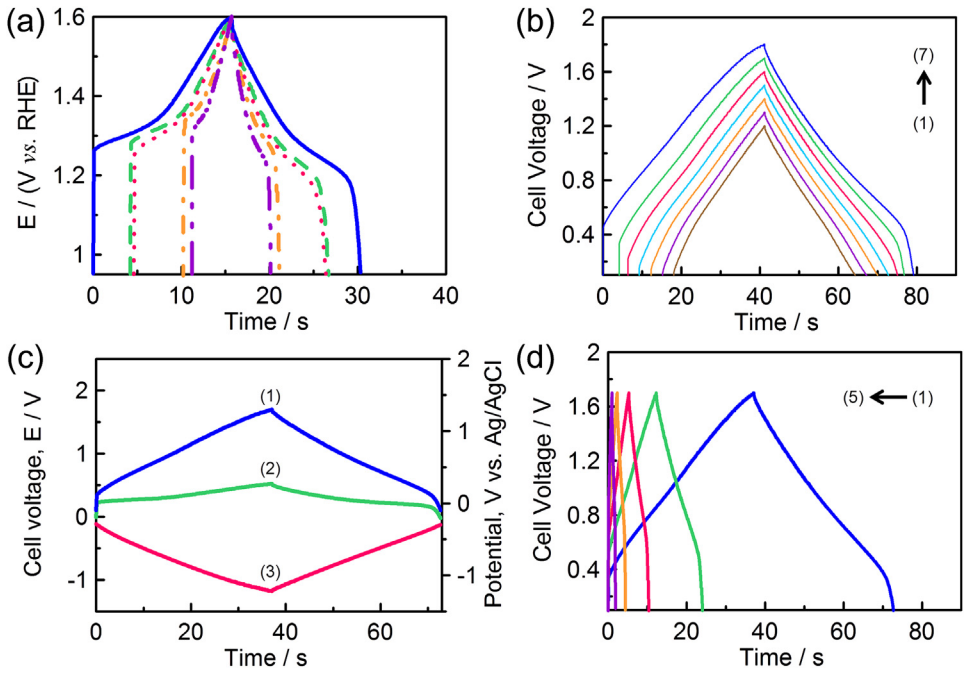

Fig. 4. (a) The three-electrode charge–discharge curves of (– · · –) $(Ni/2Co)(OH)_2$, (– · · · –) NCOH100, (–) NCOH150, (– –) NCOH200 and (· · ·) NCOH210 in 1 M NaOH at 5 mA cm^{-2}. (b) The charge–discharge curve of an asymmetric cell consisting of a NCOH150 positive electrode and an activated-carbon negative electrode measured in 1 M NaOH at 2 A g^{-1} with the cell voltage of (1) 1.2, (2) 1.3, (3) 1.4, (4) 1.5, (5) 1.6, (6) 1.7, and (7) 1.8 V. (c, 1) The two-electrode charge–discharge curve and the corresponding charges–discharge curves of (2) positive and (3) negative electrodes for an asymmetric cell consisting of a NCOH150 positive electrode and an activated-carbon negative electrode measured in 1 M NaOH at 2 A g^{-1} with the cell voltage of 1.7 V. (d) The two-electrode charge–discharge curves of an asymmetric cell consisting of a NCOH150 positive electrode and an activated-carbon negative electrode measured in 1 M NaOH at (1) 2, (2) 5, (3) 10, (4) 20, and (5) 40 A g^{-1} with the cell voltage of 1.7 V.

from 32.4 to 51.8 nm meanwhile the crystal size of hydroxides decreases from 24.2 to 17.8 nm based on the diffraction peaks centered at 38.2 and 36.7° respectively. Again, the above phenomena support the statement that the phase transformation from hydroxides to $NiCo_2O_4$ is very rapid at 210 °C under the MAHA environment. Based on the results and discussion for Figs. 1 and 5, the crystal size of $NiCo_2O_4$ and phase transformation rate can be effectively controlled by varying the MAHA temperature and time.

Based on the above viewpoint in controlling the crystal size of $NiCo_2O_4$ and phase transformation rate, a crystalline index (*CI*) is defined here to represent the phase transformation degree:

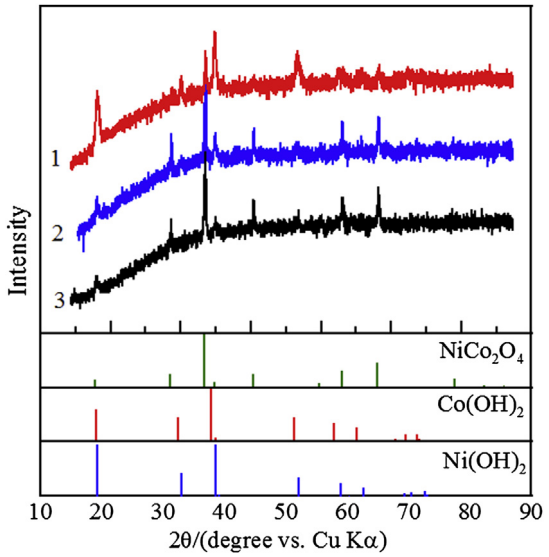

Fig. 5. XRD patterns of NCOH210 with the MAHA time equal to (1) 5, (2) 10, and (3) 15 min.

$$CI = \frac{NiCo_2O_4(311)}{(Ni/2Co)(OH)_2(001)} = \frac{I_{36.7^\circ}}{I_{38.2^\circ}} \quad (1)$$

where *I* indicates the intensity of X-ray diffraction peaks. Curves 1 and 2 in Fig. 6 show the *CI* value against the MAHA temperature and time, respectively. The *CI* value for the as-prepared participates is equal to 0 since no $NiCo_2O_4$ is formed in this sol–gel-derived binary Ni–Co hydroxide. The *CI* value is monotonously increased to 7.59 when the MAHA temperature is gradually increased to 210 °C (at a fixed MAHA time = 15 min). Similarly, the *CI* value is monotonously increased from 0.65 to 7.59 when the MAHA time is gradually increased from 5 to 15 min (at a fixed MAHA temperature = 210 °C). The above results reveal the powerful ability of MAHA for driving the phase transformation of hydroxides to crystalline oxides in comparison with a normal hydrothermal annealing process [26].

Fig. 7a and b show the typical cyclic voltammograms of NCOH210 with the MAHA time equal to 5 and 10 min, respectively. From a comparison of Figs. 7 and 3e, the CV behavior of NCOH210 with various MAHA times in the electrochemical activation process between 0.95 and 1.6 V at 25 mV s^{-1} for 150 cycles also supports our previous statements: (1) the larger crystal size of $NiCo_2O_4$ is (obtained at a longer MAHA time), the more cycles are needed to complete the electrochemical activation and (2) the larger crystal size of $NiCo_2O_4$ is, the smaller specific capacitance of NCOH210 is obtained. Furthermore, due to the significant formation of $NiCo_2O_4$ nanocrystallites for all NCOH210, the peak potentials of the redox couple on all CV curves are approximately the same. Again, the redox behavior and the utilization of electroactive species are concluded to strongly depend on the crystalline structure and crystal size of Ni–Co oxy-hydroxides.

The dependence of the specific capacitance of Ni–Co oxy-hydroxides on their *CI* value is shown in Fig. 8a. Obviously, the specific capacitance of Ni–Co oxy-hydroxides reaches a maximum value when the *CI* value is around 0.30 which corresponds to

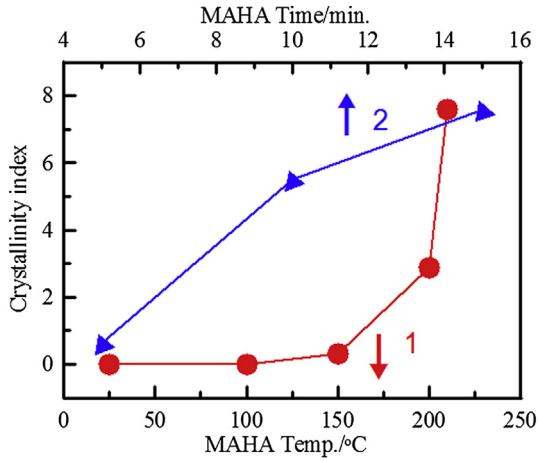

Fig. 6. The crystalline index (*CI*) value against the MAHA (1) temperature and (2) time. The MAHA time for curve 1 is fixed at 15 min and curve 2 is based on the XRD patterns of NCOH210.

NCOH150 (MAHA temperature and time respectively equal to 150 °C and 15 min). Note that as the *CI* value is not equal to zero, the average size of $NiCo_2O_4$ nanocrystals should be above 1 nm because the sub-nanometer crystallites cannot establish constructive diffraction [25]. Accordingly, the *CI* value equal to 0.30 indicates the significant growth of $NiCo_2O_4$ crystals without considering the formation of some bridging oxo bonds among certain hydroxide

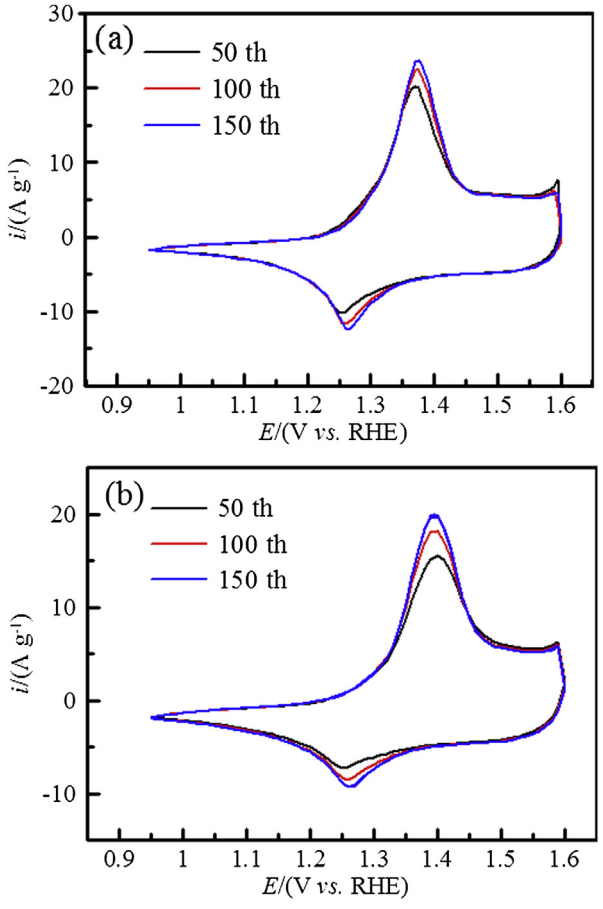

Fig. 7. The (1) 50th, (2) 100th, and (3) 150th cycles of CV curves for NCOH210 with the MAHA time equal to (a) 5 and (b) 10 min. CV were measured in 1 M NaOH at 25 mV s^{-1}.

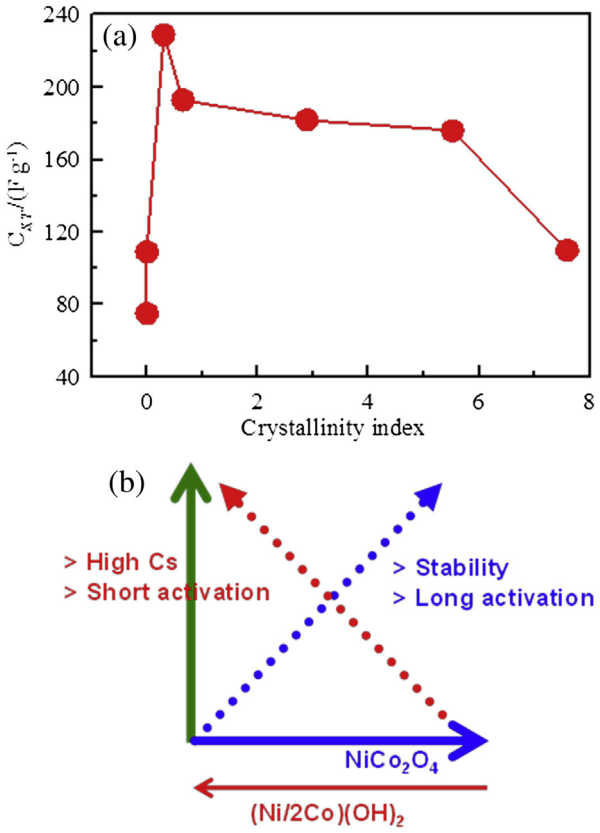

Fig. 8. (a) The dependence of the specific capacitance of Ni–Co oxy-hydroxides on the *CI* value and (b) a scheme represents the influences of phase transformation from $(Ni/2Co)(OH)_2$ to $NiCo_2O_4$ nanocrystals through the MAHA process on the capacitive performances.

precipitates. Therefore, the rapid increase of $C_{S,T}$ within a small range of *CI* (from 0 to 0.30) is understandable. Also note that there is a plateau for obtaining fairly high specific capacitance (ca. 80% of the maximum specific capacitance) when the *CI* value is between 0.65 and 5.52, which can be controlled by varying the MAHA temperature or MAHA time.

Based on all the above results and discussion, a scheme shown in Fig. 8b is used to illustrate the influences of phase transformation from $(Ni/2Co)(OH)_2$ to $NiCo_2O_4$ nanocrystals (quantified by the *CI* value) on the specific capacitance and activation time of Ni–Co oxy-hydroxides. For hydroxides derived from the sol–gel process, the hydrous and poor crystalline/amorphous nature favors the redox transitions of oxy-hydroxyl Ni and Co species. Hence, such materials only need few electrochemical activation cycles to enhance the utilization of active species although their specific capacitance depends on the intrinsic redox nature of hydroxides (e.g., bulk- and surface-active redox materials for $Ni(OH)_2$ and $Co(OH)_2$, respectively [31]). Moreover, the electrochemical stability of these hydroxides is the key issue in the supercapacitor application. On the other hand, crystalline oxides generally show a higher stability than their amorphous counterparts (e.g., Mn_3O_4 crystals vs. amorphous MnO_2 [30]). This statement is supported by the CV activation results in Fig. 3. Accordingly, the phase transformation from $(Ni/2Co)(OH)_2$ to $NiCo_2O_4$ nanocrystals is expected to promote the stability of Ni–Co oxy-hydroxides. On the other hand, crystalline oxides need many activation cycles (and long activation time) to fully utilize the electroactive species. Moreover, the growth of $NiCo_2O_4$ crystals at a longer MAHA time or a higher MAHA temperature is expected to reduce the electroactive oxy-hydroxyl-metal species involving the injecting/expelling processes of

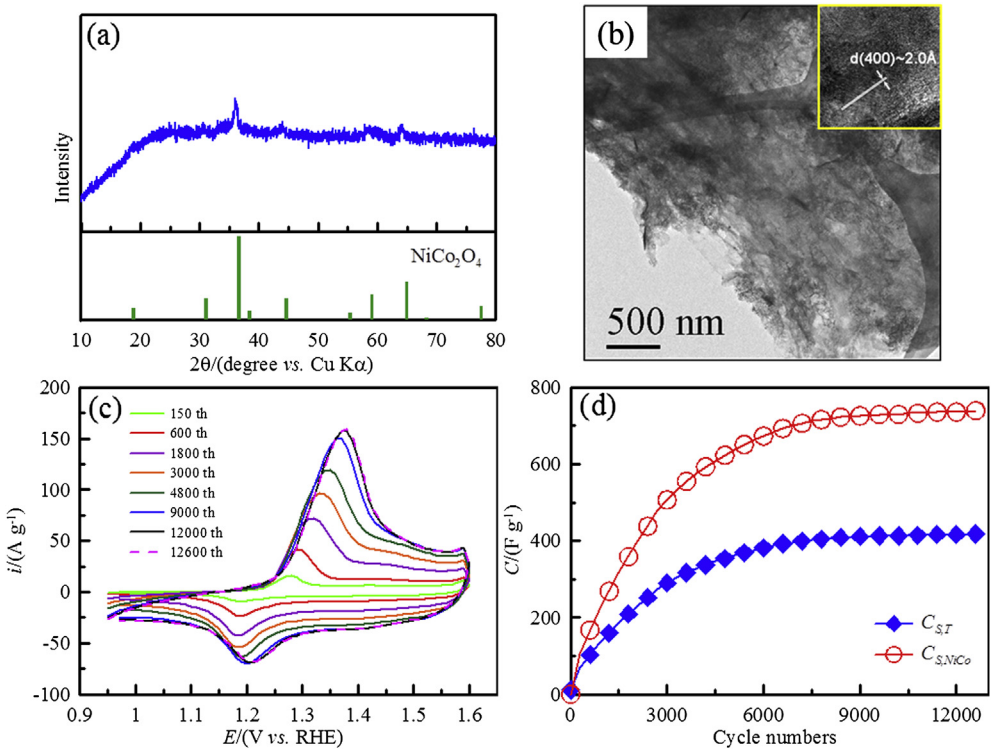

Fig. 9. (a) XRD pattern, (b) TEM image, (c) CV curves, and (d, 1) $C_{S,T}$ and (d, 2) $C_{S,NiCo}$ of a $NiCo_2O_4$/RGO composite with the MAHA temperature and time equal to 210 °C and 15 min, respectively.

electrons as well as protons, cations, or OH^- for charge storage [8,11,25] since only the electroactive species on the surface layer of anhydrous oxide crystals are freely accessible to ions. As a result, the specific capacitance of Ni–Co oxy-hydroxides prepared in this work might be significantly reduced when $NiCo_2O_4$ crystals have been significantly grown. From all the above viewpoints, an optimal degree of the phase transformation, effectively quantified by the *CI* value defined in this work, is reasonably proposed to obtain the Ni–Co oxy-hydroxides with high specific capacitance and good stability.

3.3. Effects of reduced graphene oxide in the MAHA process

Graphene has been recognized as an effective microwave absorbent for accelerating the crystallization of materials [27]. Accordingly, adding graphene oxide (GO) in the $NiCl_2{\cdot}6H_2O$–$CoCl_2{\cdot}6H_2O$ (molar ratio of 1:2) precursor solution (equal volumes of water and ethanol) is used to form a $(Ni/2Co)(OH)_2$/GO composite which is employed to obtain a well-crystalline $NiCo_2O_4$/RGO composite through the MAHA treatment. GO was prepared through the same process employed in our previous work [32]. Fig. 9 shows the XRD, TEM, CV, and specific capacitance results of a $(Ni/2Co)(OH)_2$/GO composite treated with the MAHA process at 210 °C for 15 min. Clearly, only diffraction peaks corresponding to $NiCo_2O_4$ are visible in Fig. 9a. Accordingly, GO (and RGO) is an effective microwave adsorbent to accelerate the phase transformation from the hydroxide to $NiCo_2O_4$. Therefore, the resultant composite can be denoted as $NiCo_2O_4$/RGO. Note that the peak intensity of facet (311) is very low and this peak is broad, indicating that the crystal size of $NiCo_2O_4$ is small. This statement is supported by the TEM image shown in Fig. 9b since many tiny aggregates of $NiCo_2O_4$ nanocrystals are homogeneously dispersed onto RGO nanosheets. The formation of well-crystalline $NiCo_2O_4$ is supported by the 4000-cycle of electrochemical activation (reaching 80% of the steady-state specific capacitance, see Fig. 9c and d) which is much larger than 150 cycles employed in previous sections. On the other hand, the above results demonstrate the excellent cycling stability of this $NiCo_2O_4$/RGO composite. Note that the well crystalline $NiCo_2O_4$ in the composite is of the anhydrous nature which needs much more cycles to be effectively activated. The $NiCo_2O_4$ aggregates in the composite are tiny and should exhibit a high surface/volume ratio so the utilization of $NiCo_2O_4$ is possibly enhanced although the electrochemical activation rate for such well crystalline $NiCo_2O_4$ nanocrystals by means of CV is much lower than that for Ni–Co oxy-hydroxides. Since the inner $NiCo_2O_4$ species are expected to be hard for activation (because of the difficulty of ion diffusion in the activation process), the gradual decrease in the slope of the $C_{S,T}$ vs. cycle number curve (or the $C_{S,NiCo}$ vs. cycle number curve) in the 13,000-cycle test is understandable. Moreover, due to the absence of XRD peaks corresponding to hydroxides in Fig. 9a, the *CI* value of $NiCo_2O_4$ in the composite approaches infinite. This extremely high *CI* value, of course, indicates the necessity of much more CV cycles for activating the redox species. Accordingly, *CI* is a good index quantitatively evaluating the necessity of activation cycles of Ni–Co oxy-hydroxides and $NiCo_2O_4$ prepared by the MAHA process in this work. The specific capacitance of this composite is about 410 F g^{-1} which is larger than 230 F g^{-1} for NCOH150. Moreover, the specific capacitance of $NiCo_2O_4$ estimated by equation (2) is about 730 F g^{-1}, revealing a high utilization of electroactive materials when tiny $NiCo_2O_4$ nanocrystals are evenly dispersed on the RGO nanosheets:

$$C_{S,NiCo} = \frac{C_{S,T} - C_{S,RGO}\cdot(1 - f_{NiCo})}{f_{NiCo}} \quad (2)$$

where $C_{S,T}$, $C_{S,NiCo}$, $C_{S,RGO}$, and f_{NiCo} indicate the total specific capacitance of the composite, the specific capacitance of $NiCo_2O_4$,

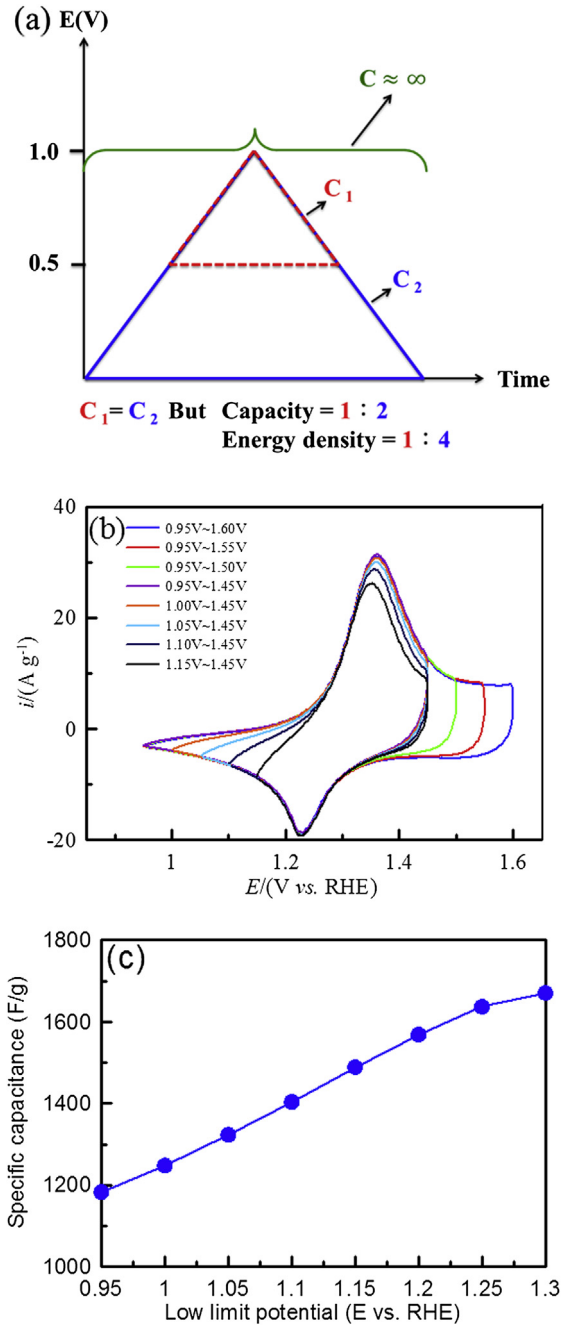

Fig. 10. (a) The charge–discharge responses of ideal electrode materials for rechargeable batteries and pseudocapacitors; (b) CV curves with changing $E_{S,U}$/$E_{S,L}$ and (c) the dependence of specific capacitance on $E_{S,L}$ measured in 1 M NaOH at 25 mV s^{-1} for a $NiCo_2O_4$/RGO composite with the MAHA temperature and time equal to 210 °C and 5 min, respectively.

the specific capacitance of RGO, and the mass fraction of $NiCo_2O_4$ within the composite, respectively. The mass fraction of $NiCo_2O_4$ was determined by the weight loss determined through the thermogravimetric analysis under an air flow from room temperature to 600 °C. Again, the energy and power densities of an asymmetric cell consisting of a positive electrode of $NiCo_2O_4$/RGO (with 4000-cycle activation) and a negative electrode of activated carbon at 40 A g^{-1} with the cell voltage 1.7 V are equal to ca. 12 Wh kg^{-1} and 42 kW kg^{-1}, respectively. These capacitive performances are better than that of a similar asymmetric cell consisting of a positive electrode of NCOH150 and a negative electrode of activated carbon.

The intrinsic properties of pseudocapacitance, especially the battery-like electrode materials, such as $Ni(OH)_2$, $Co(OH)_2$, and Ni–Co oxy-hydroxides need to be clarified since most researchers employing battery-like pseudocapacitive materials mainly focused on promoting the specific capacitance. Curves 1–3 in Fig. 10a show the charge–discharge responses of ideal electrode materials for rechargeable batteries and pseudocapacitors. Note that an ideal electrode material for rechargeable batteries will exhibit a constant charge (and discharge) potential (i.e., curve 1 with $\Delta V \approx 0$). Thus, based on the definition of capacitance (equation (3)):

$$C = \frac{it}{\Delta V} \tag{3}$$

The specific capacitance of this ideal electrode material will be infinite even though the capacity (i.e., *it*) of this electrode material may be low. Accordingly, the potential window (i.e., ΔV) employed for the calculation of specific capacitance has to be considered carefully in order to obtain the information of charge capacity. For curves 2 and 3, the slope represents the reciprocal of capacitance for two ideal pseudocapacitive materials. Since these two materials show the same slope for their charge/discharge curves but different potential windows (e.g., 0.5 and 1.0 V for curves 2 and 3, respectively), these two electrode materials show the same capacitance but the charge storage capacity and energy density ratios between curves 2 and 3 are equal to 1:2 and 1:4, respectively. Based on the above discussion, capacitor-like materials with a narrow potential window may show a high specific capacitance but a low energy density, leading to the development of asymmetric supercapacitors. This is also one of the reasons why the battery-like electrode materials are generally applied to the supercapacitor of the asymmetric type because their working voltage is usually narrow.

Fig. 10b and c show the change in the potential window of CV on the CV behavior and the specific capacitance of $NiCo_2O_4$/RGO (MAHA temperature and time equal to 210 °C for 5 min) to demonstrate the above concept. From a comparison of all curves in Fig. 10b, several features have to be mentioned. First, through the negative shift of the upper potential limit of CV ($E_{S,U}$), all CV curves follow the same trace when the potential regions of both positive and negative sweeps are overlapped. This result indicates two facts. (i) The large background current density at potentials positive than 1.45 V on both positive and negative sweeps are highly reversible. (ii) The electrochemically active species oxidized during the positive sweeps at potentials negative to 1.45 V will be completely reduced in the following negative sweeps when the lower potential limit of CV ($E_{S,L}$) is 0.95 V. The former characteristics are revealed by the highly symmetric CV responses at potentials positive than 1.45 V; i.e., this material shows an ideal capacitive behavior in this highly positive potential region. The electrochemical reversibility in this potential region is excellent for the application of the high-power supercapacitors but unfortunately, the potential window for this capacitive response is only about 0.3 V. Hence, it is suitable for the asymmetric design in order to enhance the energy density. Second, the peak current density and voltammetric charges on the positive sweeps monotonously decreases with the positive shift in $E_{S,L}$ from 0.95 to 1.15 V. However, the voltammetric responses on the negative sweeps of these CV curves follow the same trace. The former result reveals that the voltammetric current densities at potentials negative to the cathodic peak on the negative sweep are attributed to the reduction of certain active oxy-hydroxyl Ni–Co species formed in the anodic peak centered at ca. 1.36 V. The latter result suggests that the electrochemical reactions in this potential region are the same and very stable. Third, the peak potential of the anodic peak is slightly shifted with the positive shift in $E_{S,L}$ meanwhile the anodic and cathodic peaks generally shows a bell shape.

These results indicate that the reduced oxy-hydroxyl Ni–Co species formed at a more negative potential are not oxidized at a more positive or negative potential, indicating a certain degree of irreversibility for the redox couple(s). From Fig. 10c, the total specific capacitance of this composite (with 500 cycles of activation) monotonously increases from 304 to 388 F g^{-1} as $E_{S,L}$ is positively shifted from 0.95 to 1.15 V. This result indicates that a narrower potential window may significantly increase the specific capacitance but reduces the charge storage capacity of this composite. Therefore, the potential window used to evaluate/calculate the specific capacitance of pseudocapacitive materials has to be considered very carefully in order to avoid any confusion in their charge storage capacity.

4. Conclusions

The microwave-assisted hydrothermal annealing (MAHA) method has been demonstrated to be a powerful process to tune the crystal size and phase transformation degree of binary (Ni/2Co)$(OH)_2$ at relatively low annealing temperatures in a short annealing time. The phase transformation degree from (Ni/2Co)$(OH)_2$ to $NiCo_2O_4$ nanocrystals can be quantified by a crystalline index obtained from the XRD patterns. The higher content and larger size of $NiCo_2O_4$ nanocrystals are, the longer electrochemical activation time is needed. The rate of phase transformation can be enhanced by adding microwave adsorbents, graphene oxide, to obtain a $NiCo_2O_4$/RGO composite with a reduced crystal size in this work. The high specific capacitance of $NiCo_2O_4$ (about 730 F g^{-1}) indicates the high utilization of electroactive materials when tiny $NiCo_2O_4$ nanocrystals are evenly dispersed on the RGO nanosheets. Moreover, a narrower potential window may significantly increase the specific capacitance but reduce the charge storage capacity of the $NiCo_2O_4$/RGO composite, demonstrating the importance of the potential window used to obtain the specific capacitance of pseudocapacitive materials.

Acknowledgments

The financial support of this work, by the Delta-NTHU collaboration program, the National Science Council of Taiwan under NSC100-2628-E-007-028-MY2 and the boost program from Low Carbon Energy Research Center of National Tsing Hua University, is gratefully acknowledged.

References

[1] C. Li, H.P. Zhang, L.J. Fu, H. Liu, Y.P. Wu, E. Rahm, R. Holze, H.Q. Wu, Electrochim. Acta 51 (2006) 3872.
[2] Y.M. Kang, K.T. Kim, K.Y. Lee, S.J. Lee, J.H. Jung, J.Y. Lee, J. Electrochem. Soc. 150 (2003) A1538.
[3] C.C. Hu, C.Y. Cheng, J. Power Sources 111 (2002) 137.
[4] L.B. Kong, M. Liu, J.W. Lang, Y.C. Luo, L. Kang, J. Electrochem. Soc. 156 (2009) A1000.
[5] T.Y. Wei, C.H. Chen, H.C. Chien, S.Y. Lu, C.C. Hu, Adv. Mater. 22 (2010) 347.
[6] C.C. Hu, C.Y. Cheng, Electrochem. Solid-State Lett. 5 (2002) A43.
[7] C.C. Hu, K.H. Chang, T.Y. Hsu, J. Electrochem. Soc. 155 (2008) F196.
[8] B.E. Conway, Electrochemical Supercapacitors, Kluwer-Plenum Publishing Co., New York, 1999.
[9] J.W. Long, B. Dunn, D.R. Rolison, H.S. White, Chem. Rev. 104 (2004) 4463.
[10] M. Winter, R.J. Brodd, Chem. Rev. 104 (2004) 4245.
[11] K.H. Chang, Y.T. Wu, C.C. Hu, Key factors determining the performances of RuO_2-based supercapacitors, in: V. Gupta (Ed.), Recent Advances in Supercapacitors, Transworld Research Network, Kerala, India, 2006, pp. 29–56. (Chapter 3).
[12] G. Ceder, Y.M. Chiang, D.R. Sadoway, M.K. Aydinol, Y.I. Jang, B. Huang, Nature 392 (1998) 694.
[13] B. Kang, G. Ceder, Nature 458 (2009) 190.
[14] D. Wang, D. Choi, J. Li, Z. Yang, Z. Nie, R. Kou, D. Hu, C. Wang, L.V. Saraf, J. Zhang, I.A. Aksay, J. Liu, ACS Nano 3 (2009) 907.
[15] Y.S. Chen, K.H. Chang, C.C. Hu, T.T. Cheng, Electrochim. Acta 55 (2010) 6433.
[16] S. Trasatti, Electrochim. Acta 36 (1991) 225.
[17] M.R. Tarasevich, B.N. Efremov, in: S. Trasatti (Ed.), Electrodes of Conductive Metallic Oxides, Part A, Elsevier, USA, 1982, p. 227.
[18] W.K. Hu, D. Noreus, Chem. Mater. 15 (2003) 974.
[19] C. Tessier, L. Guerlou-Demourgues, C. Faure, C. Denage, B. Delatouche, C. Delmas, J. Power Sources 102 (2001) 105.
[20] C.C. Hu, C.A. Chen, J. Chin. Inst. Chem. Eng. 30 (1999) 463.
[21] J. Cheng, G.P. Cao, Y.S. Yang, J. Power Sources 159 (2006) 734.
[22] M.S. Wu, H.H. Hsieh, Electrochim. Acta 53 (2008) 3427.
[23] T.Y. Wei, C.H. Chen, K.H. Chang, S.Y. Lu, C.C. Hu, Chem. Mater. 21 (2009) 3228.
[24] K.H. Chang, C.C. Hu, Electrochem. Solid-State Lett. 7 (2004) A466.
[25] K.H. Chang, C.C. Hu, C.Y. Chou, Chem. Mater. 19 (2007) 2112.
[26] K.H. Chang, C.C. Hu, C.Y. Chou, Electrochim. Acta 54 (2009) 978.
[27] S.M. Bak, K.W. Nam, C.W. Lee, K.H. Kim, H.C. Jung, X.Q. Yang, K.B. Kim, J. Mater. Chem. 21 (2011) 17309.
[28] T.N. Ramesh, R.S. Jayashree, P. Vishnu Kamath, J. Electrochem. Soc. 150 (2003) A520.
[29] C.C. Hu, T.Y. Hsu, Electrochim. Acta 53 (2008) 2386.
[30] C.C. Hu, C.Y. Hung, K.H. Chang, Y.L. Yang, J. Power Sources 196 (2011) 847.
[31] C.C. Hu, J.C. Chen, K.H. Chang, J. Power Sources 221 (2013) 128.
[32] K.H. Chang, Y.F. Lee, C.C. Hu, C.I. Chang, C.L. Liu, Y.L. Yang, Chem. Commun. 46 (2010) 7957.